SCIENTIFIC REPORTS

OPEN

SUBJECT AREAS:
NANOBIOTECHNOLOGY
ELECTROCHEMISTRY
SENSORS AND BIOSENSORS
SMALL RNAS

Received
15 June 2012

Accepted
21 September 2012

Published
16 November 2012

Correspondence and requests for materials should be addressed to C.H.F. (fchh@sinap.ac.cn)

# DNA Nanostructure-based Interfacial engineering for PCR-free ultrasensitive electrochemical analysis of microRNA

Yanli Wen[1,4], Hao Pei[1], Ye Shen[1], Junjie Xi[2], Meihua Lin[3], Na Lu[1], Xizhong Shen[1], Jiong Li[3] & Chunhai Fan[1]

[1]Laboratory of Physical Biology, Shanghai Institute of Applied Physics, Chinese Academy of Sciences, Shanghai 201800, [2]Suzhou Institute of Nano-tech and Nano-bionics, Chinese Academy of Sciences, Suzhou 215123, [3]Zhongshan Hospital, Fudan University, Shanghai 200032, China, [4]Division of Chemistry and Ionizing Radiation Measurement Technology, Shanghai Institute of Measurement and Testing Technology, Shanghai 201203, China.

**MicroRNAs (miRNAs) have been identified as promising cancer biomarkers due to their stable presence in serum. As an alternative to PCR-based homogenous assays, surface-based electrochemical biosensors offer great opportunities for low-cost, point-of-care tests (POCTs) of disease-associated miRNAs. Nevertheless, the sensitivity of miRNA sensors is often limited by mass transport and crowding effects at the water-electrode interface. To address such challenges, we herein report a DNA nanostructure-based interfacial engineering approach to enhance binding recognition at the gold electrode surface and drastically improve the detection sensitivity. By employing this novel strategy, we can directly detect as few as attomolar (<1, 000 copies) miRNAs with high single-base discrimination ability. Given that this ultrasensitive electrochemical miRNA sensor (EMRS) is highly reproducible and essentially free of prior target labeling and PCR amplification, we also demonstrate its application by analyzing miRNA expression levels in clinical samples from esophageal squamous cell carcinoma (ESCC) patients.**

MicroRNAs (miRNAs) are endogenous, non-coding single-stranded RNAs (19~23 nucleotides) that regulate cell growth, differentiation and apoptosis at the post-transcriptional level and in a wide range. Since the discovery of miRNAs in *Caenorhabditis elegans* in 1993[1], there has been tremendous interest in studying their pivotal roles in basic biological processes of plants and animals. More recently, cumulative evidence has revealed that impaired miRNAs expression correlates with various types human cancers[2]. Significantly, some miRNAs are found to be present in serum and saliva in remarkably stable forms[3], highlighting the significance of using serum circulating miRNAs as biomarkers for early-phase cancer diagnostics and screening.

While there has been urgent need for quantitative miRNA detection both in fundamental biological studies and for diagnostic purposes, it largely remains a technical challenge due to the low abundance, short length and sequence similarity of miRNAs[4]. While northern blotting is widely accepted as the gold standard for miRNA detection and validation, the time- and labor- intensive nature of it make it inappropriate for routine applications in clinics. Quantitative polymerase chain reaction (qPCR) has become a popular method for miRNA detection. By using specially designed stem-loop structured primers, it is possible to amply short-length miRNAs from samples with high sensitivity (in the picogram range)[5]. Alternatively, miRNAs can be sensitively detected with isothermal amplification methods (e.g. rolling circle amplification, RCA) that obviate the need of temperature cycles[6,7]. In addition, hybridization-based microarray technology provides high-throughput capability for miRNA screening[8–10]. Given these advances, none of the existing methods satisfactorily meet the high standards for point-of-care testing (POCT) of miRNAs, i.e. a label-free and amplification-free method that possesses sufficiently high sensitivity and selectivity to detect very minute miRNA from serum samples, specificity to identify 1–2 mismatches in the miRNA family, and low cost and portability for applications in small clinics and/or at home.

Electrochemical sensors are well recognized to be promising POCT device due to the ready availability of inexpensive and small-size electrochemical detectors (e.g. electrochemistry-based ubiquitous glucose meters)[11–13]. However, the sensitivity of electrochemical DNA sensors is often limited by the accessibility of target DNA/RNA molecules to probes attached to the heterogeneous electrode surface due to the reduced mass transport and the presence of surface crowding effects (in contrast to probe-target recognition in homogeneous solution)[14–18]. Hence, the sensitivity of electrochemical sensors for miRNAs (pM-fM) usually does not support direct detection of low-abundance miRNAs without prior amplification with PCR. Interfacial engineering with nanostructured

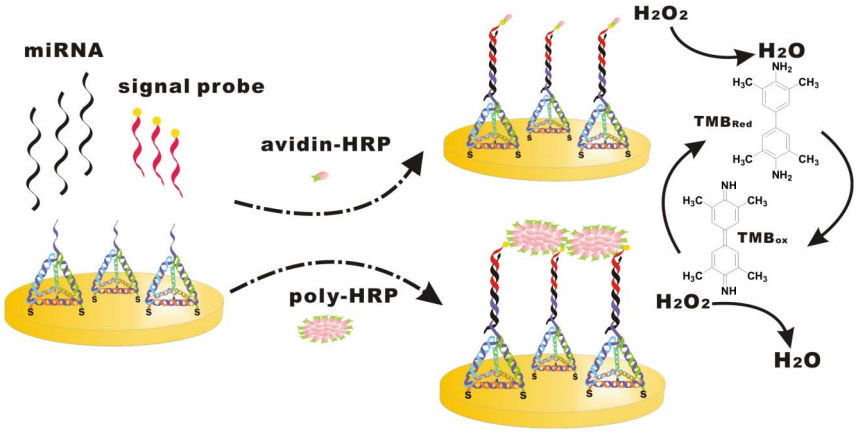


**Figure 1** | **Scheme for miRNA detection with the tetrahedron-based electrochemical miRNAs sensor (EMRS) with enzyme-based signal transduction (either avidin-HRP or high-activity poly-HRP80).**

surfaces has been theoretically and experimentally shown to greatly improve recognition abilities both thermodynamically and kinetically[15,17], which nevertheless was partially hampered by complex technologies for surface micro-/nano- fabrication. In addition, the necessity of target labeling is another barricade for POCT detection with surface-based sensors and chips[9,10].

Here we demonstrate a DNA nanostructure-based interfacial engineering strategy that provides a convenient solution to spatial control and enhanced accessibility of probes on the surface without relying on advanced micro-/nano- fabrication technologies. Due to the unmatched self-recognition properties of DNA molecules, it is possible to 'bottom-up' construct exquisite DNA nanostructures with excellent controllability and high precision arising from[19–22]. In our previous work, we have demonstrated that the use of a three-dimensional (3D) DNA tetrahedral nanostructure can improve the ability for biomolecular sensing[23,24]. By further engineering such a nanostructured surface, and adapting a base stacking-based strategy for miRNAs[9,10], we herein report an ultrasensitive electrochemical miRNA sensor (EMRS) for label-free and PCR-free detection of attomolar miRNAs with extraordinarily high sequence specificity.

## Results

"Sandwich-type" strategies are used widespread to develop various electrochemical DNA sensors[11,13]. However, it is difficult to detect miRNAs with "sandwich-type" assays due to their short length and low melting temperature. To circumvent such a problem, we herein employed a base-stacking strategy[6] to design our electrochemical miRNA sensor (EMRS). In this design, a capture DNA probe (probe 1, 10 bases) appended to one vertex of the tetrahedron-structured probe (TSP) is complementary to part of the target miRNAs (22 bases). The TSP also contains three thiol groups at the other three vertices for its immobilization at the Au surface. Our previous studies confirmed that the TSP could be rapidly self-assembled to Au and the presence of three thiol groups resulted in robust anchoring of the TSP to the Au surface, leaving the free-standing probe 1 at the top[23,25]. The surface density of TSP is typically of 8.0 pmol $cm^{-2}$. A biotin-tagged DNA strand (probe 2, 12 bases) serves as the signal probe, which is complementary to the miRNA sequence adjacent to that matches the probe 1. Hence, the three parts are held into a sandwich structure by both the base pairing between the probes and the miRNA target and the base stacking forces between the padlock probes[10]. The biotin tag at the end of the signal probe 2 can specifically bind to avidin-HRP or poly-HRP80, which catalyze the reduction of hydrogen peroxide and generate quantitative electrochemical current signals in the presence of the co-substrate, 3, 3′, 5, 5′ tetramethylbenzidine (TMB) (shown in Figure 1).

We observed two pairs of well-defined redox peaks in the cyclic voltammogram (CV) with the TSP-modified Au electrode (Figure 2A), which were assigned to the two-electron reduction and oxidation reactions of TMB. Hence, the presence of the tetrahedral nanostructure does not significantly interfere with the electron communication between TMB and the underlying Au electrode[25]. It is interesting to note that while the DNA monolayer is relatively thick (~6 nm as estimated from the duplex length), EMRS is still amenable to electrochemical transduction, possibly because DNA tetrahedra are hollow structures that allows shuttle of small molecules. This unique property makes it particularly useful for the development of high-sensitivity miRNAs sensors since it reduces the surface effect (increased layer thickness) without sacrificing electrochemical reactivity.

When the EMRS was challenged with a cancer-associated target, has-miR-21 microRNA (miR-21), we observed a typical HRP-based electrocatalytic process in CVs. The reduction peak located at ~200 mV apparently increased, resulting in a pair of asymmetric redox peaks that were characteristic of the occurrence of electrocatalysis. Apparently, miR-21 was captured onto the TSP/Au surface and formed the "sandwich" structure with the biotinylated probe 2. Subsequent binding of avidin-HRP to the biotinylated probe 2 localized the HRP enzyme to the Au electrode surface. In the presence of the electron shuttle TMB, the enzyme-catalyzed reduction of $H_2O_2$ was coupled to the electrode surface, resulting in the observed electrocatalytic peaks[23]. Amperometry provides a direct way to characterize such an HRP-catalyzed electrochemical process. Upon the onset of the potential at 100 mV, we instantly observed a current (I)-versus-time (t) decay curve, which reached a plateau (steady-state current) within ~100 s (Figure 2B). The background current of EMRS was as low as ~15 nA, suggesting the absence of major

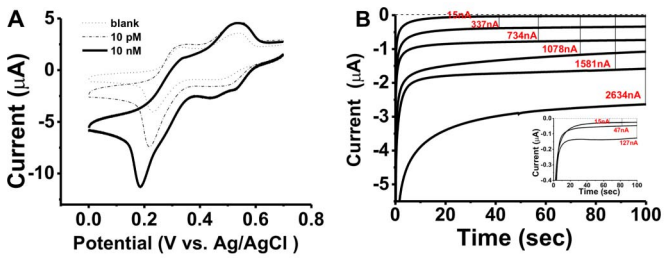


**Figure 2** | **(A) Cyclic voltammograms for EMRS in the absence (---)and presence of 10 pM (····) and 10 nM miR-21(—).** Scan rate: 100 mV/s. (B) Amperometric curves (i-t) for EMRS tested with a series of miR-21 concentrations. From top to bottom: 0, 1 pM, 10 pM, 100 pM, 1 nM, 10 nM. Insert shows the low concentration range of the i-t curves for 10 fM and100 fM miR-21. The potential was held at 100 mV.

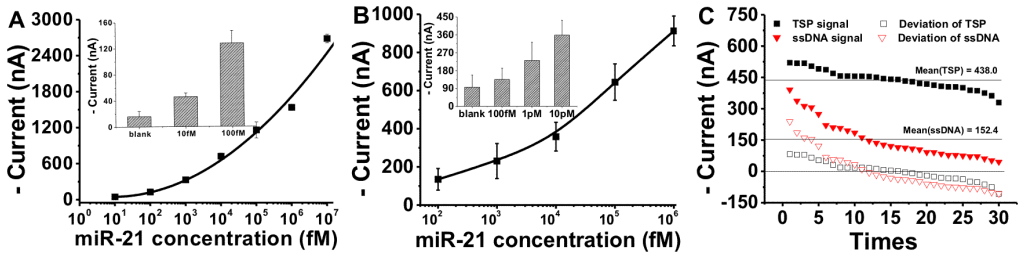


**Figure 3 | Logarithmic plot of amperometric current vs miR-21 concentration for (A) EMRS and (B) ssDNA probe-based sensor.** Error bars represent standard deviations for measurements taken from at least three independent experiments. (C) Comparison of reproducibility between EMRS and ssDNA-based sensor by testing over 30 times for miR-21 (10 pM). Standard deviations for both sensors stand for the difference between the real current and mean current.

non-specific binding (NSB) of HRP. Significantly, when the miR-21 target of 10 nM was added to the solution, the electrochemical current signal reached 2634 nA, representing a very high signal-to-background ratio of 175. We then challenged the EMRS with a series of concentrations of the synthetic miR-21 target in the range from 10 fM to 10 nM. The amperometric signal increased monotonically with the logarithm concentration of miR-21, resulting in a typical dose-response curve (Figure 3A). The detection limit of EMRS was determined to be 10 fM as the electrochemical signal for 10 fM miR-21 was still significantly larger than the background (>3 SD; Figure 3A, inset).

To further substantiate the advantages of using 3D TSP, we designed a control system using thiolated single-stranded capture probe 1 (SH-ss-miR-21) that was directly anchored to Au electrodes. Similarly, sandwich assays were established by using SH-ss-miR-21 probe 1 and biotinylated signal probe 2 (swRP-miR-21) that flanked the target miR-21. Avidin-HRP was also employed to generate electrocatalytic signals. The surface density was tuned to be roughly the same as that for the TSP-modified surface (8.0 pmol $cm^{-2}$) by changing the concentration of the probe 1 in the assembly solution. This type of sensors shows much poorer performance than the TSP-based EMRS (Figure 3B). The background current was significantly increased to ~ 96 nA (as compared to ~15 nA in EMRS), reflecting enhanced NSB of the enzyme. The signal for 1 nM of miR-21 was ~912 nA, corresponding to a signal-to-background ratio of ~9, which was more than an order of magnitude smaller than that for EMRS (~100). Also, when miR-21 concentration was lower than 10 pM, the signal was indistinguishable from the background (<3 SD). Hence, the sensitivity of ssDNA probe-based sensors was lower than that of EMRS by approximately three orders of magnitude. In addition, the reproducibility of both sensors was evaluated by testing them over 30 times for 10 pM of miR-21 (Figure 3C). We found that the standard deviation (SD) for TSP-based EMRS (~47.1) was 2-fold lower than that for ssDNA-based sensors (~92.9). This suggests that EMRS possesses much higher reproducibility than ssDNA probe-based sensors, an effect arising from the highly reproducible surface assembly process with TSP.

To meet high-end requirements for the detection of low-abundance miRNAs, we attempted to further improve the sensitivity of EMRS by employing poly-HRP80, a polymerized streptavidin-HRP conjugate with up to 400 HRP molecules per conjugate. Poly-HRP80 is known to be of high catalytic activity, which nevertheless often increases the background as well due to the presence of significant NSB. Given the high protein resistance ability of DNA nanostructure-decorated surfaces,[23] we expected that poly-HRP80 could amplify the electrochemical signal without significantly increasing the background current. Indeed, we found that the background almost remained the same while the signal was greatly enhanced with the use of poly-HRP80 (Figure 3A and Figure 4A). As a comparison, the signal became indistinguishable with the background when avidin-HRP was employed for the detection of miR-21 of <10 fM; while the poly-HRP80-based EMRS could detect as few as 10 aM miRNAs (~600 molecules in 100 μL). Hence, the sensitivity has been improved by three orders of magnitude. Moreover, poly-HRP80-based EMRS had an extremely large dynamic range, covering nine orders of magnitude.

The electrochemical signal of EMRS was optimized in terms of hybridization temperature and time (see Fig. S1 in the SI). Particularly, we found that sensing performance of EMRS was critically dependent on the surface density of TSP. When the surface density was increased by increasing the assembly concentration of TSP from 1 μM to 2 μM, the electrochemical signal was decreased by ~10% while the background was suppressed by ~40%. The latter suggests that high packing density can reduce NSB of HRP at the surface. In order to avoid possible interference of DNA hybridization due to increased surface crowding (e.g. 10% decrease of the signal), we introduced thiolated DNA tetrahedral structure free of the pendant probe (TS), and engineered the inter-strand spacing by tuning the ratio of TS and TSP (Figure 4B). Significantly, we found that the signal-to-noise ratio for miRNA targets could be further improved with this dilution strategy. By changing the ratio of TSP/TS from 1:0 to 1:10, the electrochemical signal for 10 aM miR-21 was increased by ~3 fold while the background nearly remained the same, suggesting that the sensitivity of EMRS could be further improved with this surface engineering strategy. Further dilution of TSP with TS resulted in decreased signals, an effect arising from the significant loss of surface-confined probes. Interestingly, this dilution-based enhancement effect was not observed for miRNA of relatively high concentrations (e.g. 1 fM). This is possibly because poly-HRP80 is a very large structure, and the accessibility is limited when the surface is crowded at relatively high target concentrations.

The specificity of EMRS was tested by using a family of human let-7 sequences of 1 pM possessing closely related sequences with high homology (variation of only 1-3 nt)[26]. Importantly, we found that EMRS with the probe designed for let-7d generated much higher signals for let-7d than other let-7 miRNAs and non-cognate sequences (usually by 1-2 orders of magnitude, $P<0.05$, Figure 4C). In fact, even let-7a and let-7e containing G/T substitutions that are known to have relatively high binding energy[27,28], led to signals at least 3-fold smaller than that for let-7d. This high mismatch discrimination ability reflects the high specificity offered by the nanostructured probes at the Au surface.

EMRS can also effectively differentiate precursor miRNAs (pre-miRNAs) from mature ones. Pre-miRNAs are spliced in vivo to from mature miRNAs, which are then assembled into active RNA-induced silencing complexes (RISCs)[2]. Their co-existence often results in false-positives in medical assays[10]. We then challenged EMRS with a hairpin-structured precursor human miRNA, pre-miR-31[29], and mature miR-31 sequences. Significantly, the signal for the precursor was nearly 2 orders of magnitude lower than that for mature miR-31 (Figure 4D), suggesting that EMRS can suppress the signal for pre-miRNAs and realize error-free detection of miRNAs.

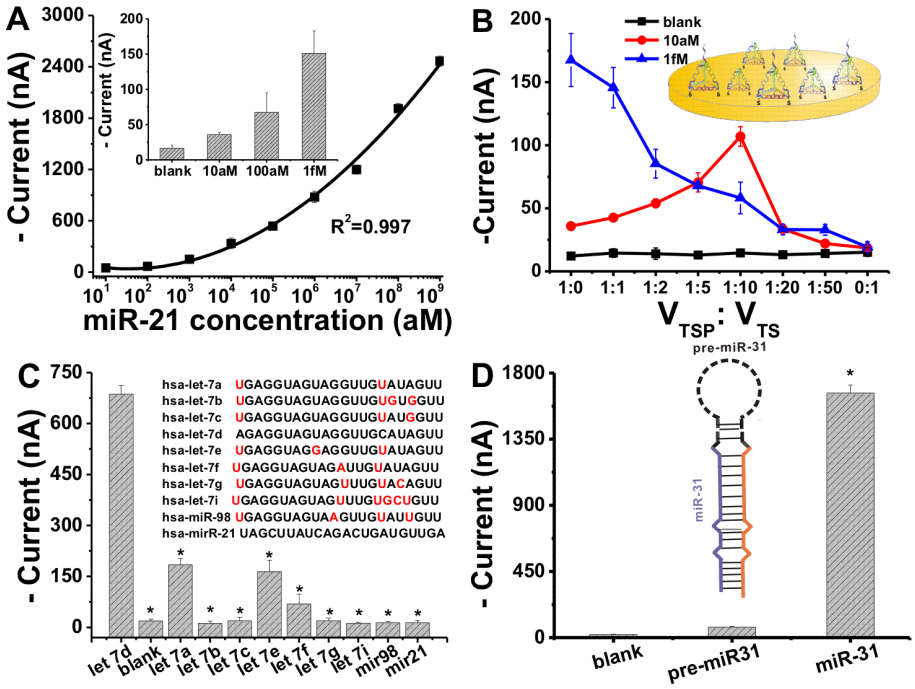


**Figure 4 | Sensitivity and specificity of the tetrahedra-based EMRS with poly-HRP80 amplification.** (A) Logarithmic plot of amperometric current vs miR-21 concentration for tetrahedra-based EMRS with poly-HRP amplification. Insert shows the low concentration range of miR-21. Corresponding amperometric curves are shown in Fig. S3. Error bars represent standard deviations for measurements taken from at least three independent experiments. (B) Effect of hybridization efficiency by tuning the ratio of TS and TSP while maintaining the total concentration of DNA tetrahedral in the assembly solution (1 μM). (C) Discrimination of let 7 family members, miR-21 used as negative control (all of 1 pM), * $P < 0.05$ significantly different from the let-7d, and (D) Pre-/mature miRNA discrimination (of 10 pM), * $P < 0.05$ significantly different from the pre-miR-31 and blank. Error bars represent standard deviations for measurements taken from at least three independent experiments.

Given the ultrahigh sensitivity and excellent sequence specificity of EMRS, we attempted to analyze expression levels of miRNAs in real samples. Hsa-let-7d miRNA in total RNAs extracted from tumoral and normal tissues of human liver, lung and prostate were first employed. We found that the expression levels of hsa-let-7d in tumoral tissues were significantly lower than that in normal tissues ($P<0.05$; Figure 5A). This observation of downregulated expression of hsa-let-7d in tumoral tissues correlates well with the previously reported literature[2,26]. Due to its high sensitivity, EMRS-based profiling could be performed with only 100 ng of total RNA (Figure 5B). We next challenged EMRS for detection of miR-21 in clinical samples of esophageal squamous cell carcinoma (ESCC). Total RNAs (100 ng) were extracted from esophageal tumoral tissue and adjacent normal tissues collected from six ESCC patients. Figure 5C shows that the miR-21 expressional levels in the ESCC tumoral tissues were systematically higher than those in adjacent normal tissues, suggesting an up-regulation of miR-21 expression in the tumoral tissue. Collectively, the mean level of miR-21 was increased by a factor of 2.5 in the esophageal tumor tissues compared with the adjacent normal tissues ($P<0.05$), which was similar to the literature value of 2∼4 fold change in ESCC tumoral tissue versus normal tissues[30,31].

## Discussion

DNA hybridization at the Au surface is often hampered by target accessibility and mass transport[14]. While thiolated ssDNA-modified Au surfaces have been popularly employed to develop DNA sensors and devices, more recent evidence has shown that ssDNA probes are in fact not uniformly distributed at the surface[32,33]. For example,

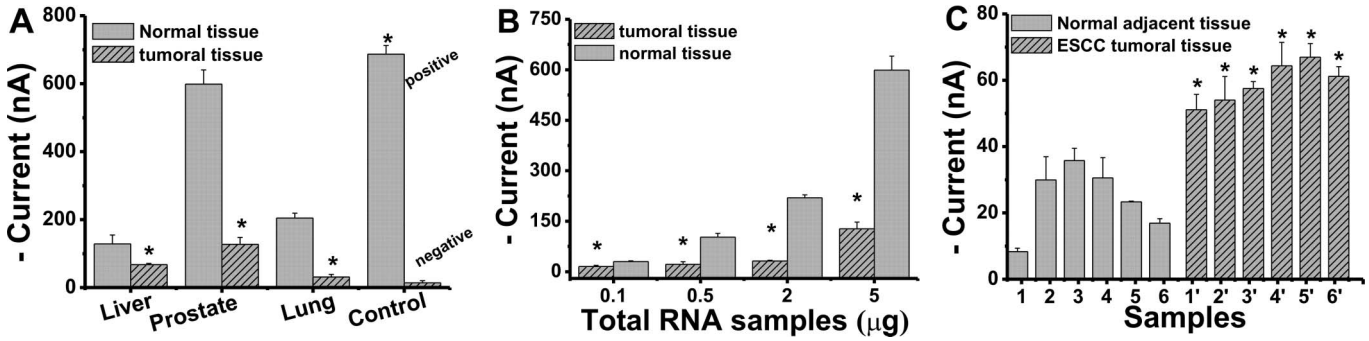


**Figure 5 |** (A) Signals of EMRS for let-7d in total RNAs (5.0 μg) extracted from liver, lung and prostate tissues. Synthetic let-7d (1 pM) was used as positive control and the negative control was the signal obtained in the absence of total RNAs. (B) Detection of let-7d with EMRS using different amount of total RNAs from prostate tumoral tissue and normal tissue. (C) Detection of miR-21 with EMRS in the total RNA of esophageal squamous cell carcinoma (ESCC) patients (all of 100 ng). Statistical analysis was performed by paired t-test. * $P < 0.05$ significantly different from relative normal tissue. Error bars represent standard deviations for measurements taken from at least three independent experiments.

atomic force microscopic (AFM) studies provided direct evidence of the presence of clustered ssDNA at the Au surface[32], which possibly arises from aggregation during the self-assembly and inter-strand entanglement of these soft polymer[34–38]. The rigid DNA tetrahedral nanostructures clearly provide a solid base for DNA probes with the precise 1:1 ratio, which are spatially isolated by the bulky nanostructure[23,39,40]. Further engineering of the interface by using diluting TS nanostructure (free of the probe) results in surfaces with extremely sparse DNA probes that may minimize the surface crowding effect and increase the target accessibility[14,41]. On the other hand, previous theoretical and experimental studies have revealed that diffusion and convection of analytes are usually facilitated at nanostructured surfaces[14,18,42,43]. While direct evidence is not available due to the absence of appropriate characterization techniques, EMRS's ability to detect down to aM miRNAs implies that the mass transport is also enhanced at DNA nanostructure-modified surfaces.

The 3D DNA nanostructure-based EMRS thus provides an ultrasensitive approach for reliable quantitative detection of attomolar miRNAs with extraordinarily high sequence specificity. Compared to previously reported electrochemical DNA sensors, EMRS shows several combined advantages. First, DNA probes are uniformly distributed on spatially isolated DNA tetrahedral nanostructures that minimize inter-strand interactions and facilitate hybridization[23]. Also, the relatively large nanostructure places the probes 6 nm over the Au surface, making them stay in a solution-like environment. Second, DNA tetrahedra-modified surfaces are inherently protein-resistant[23], which greatly minimizes the background and allows high signal amplification with poly-HRP80 without sacrificing the signal-to-background ratio. Third, the very rigid structure of DNA tetrahedra and the presence of three thiols per nanostructure result in highly stable and reproducible self-assembled nanostructure surfaces, contributing to both the low background and small electrode-to-electrode variation. Finally, given that EMRS is based on normal Au surfaces, it is fully compatible with the low-cost screen printed electrode technology and easily scalable for mass production of sensors. When coupled with portable electrochemical detectors, EMRS can provide a solution to directly detecting miRNA biomarkers in the POCT setting, which is otherwise difficult with qPCR or other solution-phase amplification methods[44].

Because of the presence of these properties, EMRS has a remarkably high signal-to-background ratio of more than 100, excelling most previously reported high-sensitivity DNA sensors (typically 3–10)[43,45]. The ultrahigh attmolar sensitivity of EMRS permits direct detection of low-abundance miRNA biomarkers (down to ~600 copies) without prior PCR amplification, a highly desirable property for miRNA-based diagnostics. The sensitivity of EMRS compares favorably with many previously reported surface-based nucleic acid sensors that rely on either complicated lithography-based surface nanofabrication technologies or expensive readout (e.g. AFM). In addition, the use of stacking probes also offers very high specificity for effective differentiation of ho mologous miRNAs with even 1-base mismatches[10]. With this design, pre-miRNAs that often co-exist with miRNAs can also be easily distinguished, which was otherwise difficult with qPCR.

Dynamic range is another important factor for practical clinical assays. Many sensitive sensing technologies are inherently limited by their small dynamic ranges (even as low as 1–2 logs)[43], which often complicate single-plex assays (with unnecessary serial dilutions) and largely hamper the performance of multiplex detection. Significantly, the impressive dynamic range of 9 orders of magnitude of EMRS enables simultaneous target quantification ranging from low attomolar concentrations to 10 nM or even higher, providing an unprecedented opportunity to screen miRNAs that often exist very diversely in cells (ranging from ~10–50, 000 copies/cell)[5].

To conclude, DNA nanostructure-based interface engineering offers a combination of desirable advantages for sensitive and reliable quantification of miRNAs. Also importantly, while detection abilities of bioassays are often hampered in real, complex biological samples, EMRS has demonstrated excellent real applicability by its performance in analysis of clinical samples. EMRS is also essentially free of tedious target labeling with enzymes, a common practice that is often employed in various detection methods (e.g., qPCR and microarrays). By using inexpensive electrodes and portable electrochemical detectors, we expect that this highly sensitive DNA nanotechnology-based EMRS can satisfy the needs of POCT, and become a promising miRNA quantification method in clinical diagnosis.

## Methods

**Materials.** All oligonucleotides, including miRNAs and DNA probes, were synthesized and purified by Invitrogen, and the sequences are shown in Table S1. Total RNAs from tumor tissue and normal adjacent tissue in three human organs (liver, prostate and lung) were purchased from Ambion (Houston, Texas), and were used without further fractionation or enrichment. Total RNA samples from esophageal squamous cell carcinoma (ESCC) patients were provided by Zhongshan Hospital of Shanghai. Written informed consents of all donators were obtained and approval was received for our study from the local Ethics Committee on Human Research.

The TMB substrate (TMB=3, 3′, 5, 5′ tetramethylbenzidine) was purchased from Neogen in the format of a ready-to-use reagent (K-blue low activity substrate, $H_2O_2$ included). Horseradish peroxidase-conjugated avidin (avidin-HRP) was from Roche Diagnostics. Streptavidin-Poly-HRP80 (poly-HRP80) and poly-HRP diluent were obtained from Fitzgerald Industries International (Acton, MA). Poly-HRP80 is a supermolecular enzyme complex containing up to 400 (80*5) HRP molecules while avidin-HRP only contains ~20 HRP molecules. Ethylene glycol-terminated thiol ($HS\text{-}(CH_2)_{11}\text{-}EG_2\text{-}OH$, OEG) was purchased from Prochimia (Poland). Tris (2-carboxyethyl) phosphine hydrochloride (TCEP) and diethyl pyrocarbonate (DEPC) were from Sigma. All other chemicals were of analytical grade and all chemicals were used without further purification. All solutions were prepared with RNase-free water. The RNase-free water was prepared with Milli-Q water (18 MΩ · cm resistivity) treated with 0.1% DEPC.

**Cleaning and modification of gold electrode surfaces.** Gold electrodes (2 mm in diameter) were cleaned following the reported protocol[11]. Tetrahedral nanostructure-based capture probes (TSP) for miRNA detection (tetra-miR-21) were formed and the surface density was measured as previously reported[23]. Four strands, tetra-miR-21, B, C, D were dissolved in TE buffer (10 mM Tris, 1 mM EDTA, pH 8.0) with a final concentration of 50 μM. 1 μL of each strand was mixed with 5 μL of TCEP (30 mM) and 41 μL of TM buffer (20 mM Tris, 50 mM $MgCl_2$, pH 8.0). The resulting mixture was heated to 95°C for 2 min, and then cooled to 4 °C over 30 s using a Peltier thermal cycler PTC-200 (MJ. Research Inc., SA). After that, 3 μL of TSP (1 μM) were pipetted to the cleaned gold electrode and incubated overnight at room temperature. The self-assembly process of the tetra-let-7d probe was the same as that of the tetra-miR-21 one. The thiolated single-stranded (ss-) miR-21 capture probe 1 (SH-ss-miR-21) was immobilized to Au electrodes in the TM buffer (20 mM Tris, 50 mM $MgCl_2$, pH 8.0). 3 μL of 0.2 μM SH-ss-miR-21 probes were pipetted to the surface of gold electrode and incubated for 3 hours at room temperature and then the SH-ss-miR-21 modofied electrode was further treated with 2 mM OEG overnight to obtain well aligned DNA monolayers. The resulting electrodes were rinsed with 0.01 M phosphate buffered saline (PBS, prepared with RNase-free water) and dried lightly with $N_2$ before hybridization.

**MiRNA detection with EMRS.** MiRNA detection was carried out in the sandwich assay format. All the sequences of mature human miRNAs are listed in Table S2. The synthetic target miR-21 was first mixed with the biotinylated signal probe 2 (swRP-miR-21, 500 nM) in 100 μL of 10 mM phosphate buffer (PB) with 1 M NaCl and 20 mM $MgCl_2$ (pH 7.4) and heated to 80 °C for 5 min. The mixture was cooled to room temperature for more than 20 min, and then the mixture was added to a 2 mL RNase-free microtube (Axygen). Finally, the tetra-miR-21 probes modified electrode was incubated in the 100 μL solution in the microtube for hybridization. After 5-hr incubation at 10 °C, the electrode was rinsed with 0.01 M PBS buffer and then incubated with 3 μL of avidin-HRP (0.5 U/mL) or poly-HRP80 (1 μg/mL) for 15 min at 4 °C in the refrigerator. The sensor was then extensively rinsed with 0.01 M PBS and subjected to electrochemical measurements. The detection of let-7 family and real miRNA samples was performed with the same protocol.

**Electrochemical Measurements.** Electrochemical measurements were performed with a CHI 630 electrochemical workstation (CH Instruments Inc., Austin) and a conventional three-electrode configuration was employed all through the experiment, which involved a gold working electrode, a platinum wire auxiliary electrode, and an Ag/AgCl (3 M KCl) reference electrode. Cyclic voltammetry was carried out at a scan rate of 100 mV/s. Amperometric detection was fixed at 100 mV and the electrocatalytic reduction current was measured at 100 s after the HRP redox reaction reached the steady state.

1. Lee, R. C., Feinbaum, R. L. & Ambros, V. The C. elegans heterochronic gene lin-4 encodes small RNAs with antisense complementarity to lin-14. *Cell* **75**, 843–854 (1993).

2. Esquela-Kerscher, A. & Slack, F. J. Oncomirs - microRNAs with a role in cancer. *Nature Rev. Cancer* **6**, 259–269 (2006).
3. Mitchell, P. S. *et al*. Circulating microRNAs as stable blood-based markers for cancer detection. *Proc. Natl. Acad. Sci. USA* **105**, 10513 (2008).
4. Cissell, K. A., Shrestha, S. & Deo, S. K. MicroRNA detection: challenges for the analytical chemist. *Anal. Chem.* **79**, 4754–4761 (2007).
5. Chen, C. *et al*. Real-time quantification of microRNAs by stem–loop RT–PCR. *Nucleic Acids Res.* **33**, e179–e179 (2005).
6. Zhou, Y. *et al*. A dumbbell probe-mediated rolling circle amplification strategy for highly sensitive microRNA detection. *Nucleic Acids Res.* **38**, e156 (2010).
7. Jia, H., Li, Z., Liu, C. & Cheng, Y. Ultrasensitive detection of microRNAs by Exponential isothermal amplification. *Angew. Chem. Int. Ed.* **49**, 5498–5501 (2010).
8. Thomson, J. M., Parker, J., Perou, C. M. & Hammond, S. M. A custom microarray platform for analysis of microRNA gene expression. *Nature Methods* **1**, 47–53 (2004).
9. Git, A. *et al*. Systematic comparison of microarray profiling, real-time PCR, and next-generation sequencing technologies for measuring differential microRNA expression. *RNA* **16**, 991–1006 (2010).
10. Duan, D. *et al*. Label-free high-throughput microRNA expression profiling from total RNA. *Nucleic Acids Res.* **39**, e154 (2011).
11. Zhang, J., Song, S. P., Wang, L. H., Pan, D. & Fan, C. H. A gold nanoparticle-based chronocoulometric DNA sensor for amplified detection of DNA. *Nature Protoc.* **2**, 2888–2895 (2007).
12. Xiang, Y. & Lu, Y. Using personal glucose meters and functional DNA sensors to quantify a variety of analytical targets. *Nature Chem.* **3**, 697–703 (2011).
13. Zuo, X., Xiao, Y. & Plaxco, K. High specificity, electrochemical sandwich assays based on single aptamer sequences and suitable for the direct detection of small-molecule targets in blood and other complex matrices. *J. Am. Chem. Soc.* **131**, 6944–6945 (2009).
14. Gong, P. & Levicky, R. DNA surface hybridization regimes. *Proc. Natl. Acad. Sci.* **105**, 5301–5306 (2008).
15. Squires, T. M., Messinger, R. J. & Manalis, S. R. Making it stick: convection, reaction and diffusion in surface-based biosensors. *Nature Biotechnology* **26**, 417–426 (2008).
16. Wu, J., Campuzano, S., Halford, C., Haake, D. A. & Wang, J. Ternary Surface Monolayers for Ultrasensitive (Zeptomole) Amperometric Detection of Nucleic Acid Hybridization without Signal Amplification. *Analytical Chemistry* (2010).
17. Soleymani, L., Fang, Z. C., Sargent, E. H. & Kelley, S. O. Programming the detection limits of biosensors through controlled nanostructuring. *Nature Nanotechnol.* **4**, 844–848 (2009).
18. Yang, H. *et al*. Direct, Electronic MicroRNA Detection for the Rapid Determination of Differential Expression Profiles. *Angew. Chem. Int. Ed.* **48**, 8461–8464 (2009).
19. Seeman, N. DNA in a material world. *Nature* **421**, 427–431 (2003).
20. Yan, H. MATERIALS SCIENCE: Nucleic Acid Nanotechnology. *Science* **306**, 2048–2049 (2004).
21. Andersen, E. S. *et al*. Self-assembly of a nanoscale DNA box with a controllable lid. *Nature* **459**, 73–76 (2009).
22. Goodman, R. P. *et al*. Rapid chiral assembly of rigid DNA building blocks for molecular nanofabrication. *Science* **310**, 1661–1665 (2005).
23. Pei, H. *et al*. A DNA Nanostructure-based Biomolecular Probe Carrier Platform for Electrochemical Biosensing. *Adv. Mater.* **22**, 4754–4758 (2010).
24. Mitchell, N. *et al*. A DNA Nanostructure for the Functional Assembly of Chemical Groups with Tunable Stoichiometry and Defined Nanoscale Geometry. *Angew. Chem. Int. Ed.* **48**, 525–527 (2009).
25. Wen, Y. *et al*. DNA Nanostructure-Decorated Surfaces for Enhanced Aptamer-Target Binding and Electrochemical Cocaine Sensors. *Anal. Chem.* (2011).
26. Roush, S. & Slack, F. J. The let-7 family of microRNAs. *Trends Cell Biol.* **18**, 505–516 (2008).
27. Lee, I. *et al*. Discriminating single-base difference miRNA expressions using microarray Probe Design Guru (ProDeG). *Nucleic Acids Res.* **36**, e27 (2008).
28. Neely, L. A. *et al*. A single-molecule method for the quantitation of microRNA gene expression. *Nature Methods* **3**, 41 (2006).
29. Lund, E., Guttinger, S., Calado, A., Dahlberg, J. E. & Kutay, U. Nuclear export of microRNA precursors. *Science* **303**, 95–98 (2004).
30. Ogawa, R. *et al*. Expression profiling of micro-RNAs in human esophageal squamous cell carcinoma using RT-PCR. *Med. Mol. Morphol.* **42**, 102–109 (2009).
31. Feber, A. *et al*. MicroRNA expression profiles of esophageal cancer. *J. Thorac. Cardiovasc. Surg.* **135**, 255–260 (2008).
32. Josephs, E. A. & Ye, T. A Single-Molecule View of Conformational Switching of DNA Tethered to a Gold Electrode. *J. Am. Chem. Soc.* **134**, 10021–10030 (2012).
33. Ricci, F. *et al*. Surface chemistry effects on the performance of an electrochemical DNA sensor. *Bioelectrochemistry* **76**, 208–213 (2009).
34. Wong, E. L. S., Chow, E. & Gooding, J. J. DNA recognition interfaces: The influence of interfacial design on the efficiency and kinetics of hybridization. *Langmuir* **21**, 6957–6965 (2005).
35. Irving, D., Gong, P. & Levicky, R. DNA Surface Hybridization: Comparison of Theory and Experiment. *J. Phys. Chem.-B* **22**, 7631–7640 (2010).
36. Wong, I. Y. & Melosh, N. A. *Biophys. J.* **98**, 2954–2963 (2010).
37. Fan, C. H., Plaxco, K. W. & Heeger, A. J. Electrochemical interrogation of conformational changes as a reagentless method for the sequence-specific detection of DNA. *Proc. Natl. Acad. Sci.* **100**, 9134–9137 (2003).
38. Zhang, J., Song, S. P., Wang, L. H., Pan, D. & Fan, C. H. A gold nanoparticle-based chronocoulometric DNA sensor for amplified detection of DNA. *Nat. Protoc.* **2**, 2888–2895 (2007).
39. Pei, H. *et al*. Regenerable electrochemical immunological sensing at DNA nanostructure-decorated gold surfaces. *Chem. Commun.* **47**, 6254–6256 (2011).
40. Wen, Y. L. *et al*. DNA Nanostructure-Decorated Surfaces for Enhanced Aptamer-Target Binding and Electrochemical Cocaine Sensors. *Analytical Chemistry* **83**, 7418–7423 (2011).
41. Lu, N. *et al*. Charge transport within a three-dimensional DNA nanostructure framework. *J. Am. Chem. Soc.* **134**, 13148–13151 (2012).
42. Squires, T. M., Messinger, R. J. & Manalis, S. R. Making it stick: convection, reaction and diffusion in surface-based biosensors. *Nat. Biotechnol.* **26**, 417–426 (2008).
43. Soleymani, L., Fang, Z., Sargent, E. H. & Kelley, S. O. Programming the detection limits of biosensors through controlled nanostructuring. *Nature Nanotechnol.* **4**, 844–848 (2009).
44. Cheng, Y. Q. *et al*. Highly Sensitive Determination of microRNA Using Target-Primed and Branched Rolling-Circle Amplification. *Angew. Chem. Int. Ed.* **48**, 3268–3272 (2009).
45. Soleymani, L. *et al*. Nanostructuring of patterned microelectrodes to enhance the sensitivity of electrochemical nucleic acids detection. *Angew. Chem. Int. Ed.* **48**, 8457–8460 (2009).


## Acknowledgements

This work was supported by Ministry of Science and Technology (MOST 2012CB932600), National Science Foundation of China (NSFC 91123037, 90913014) and Chinese Academy of Sciences (KJCX2-EW-N03).

## Author contributions

CF, YW and HP designed the experiments and wrote the main manuscript text, YW, HP, YS JX, ML, NL performed experiments, and XS and JL provided sampels. All authors reviewed the manuscript.

## Additional information

**Supplementary information** accompanies this paper at http://www.nature.com/scientificreports

**Competing financial interests:** The authors declare no competing financial interests.



**How to cite this article:** Wen, Y. *et al*. DNA Nanostructure-based Interfacial engineering for PCR-free ultrasensitive electrochemical analysis of microRNA. *Sci. Rep.* **2**, 867; DOI:10.1038/srep00867 (2012).